EPJ Web of Conferences **91**, 00007 (2015)
DOI: 10.1051/epjconf/20159100007

Auger yield calculations for medical radioisotopes

Boon Q. Lee[1,a], Tibor Kibédi[1], and Andrew E. Stuchbery[1]

[1] *Department of Nuclear Physics, The Australian National University, ACT 2601, Australia*

Abstract. Auger yields from the decays of ^{71}Ge, ^{99m}Tc, ^{111}In and $^{123-125}$I have been calculated using a Monte Carlo model of the Auger cascade that has been developed at the ANU. In addition, progress to improve the input data of the model has been made with the Multiconfiguration Dirac-Hartree-Fock method.

1 Introduction

Radiolabelled molecules are used in targeted tumour therapy as they can selectively deliver high doses to the cancer cells. In these molecules, antibodies and antibody fragments as well as peptides are used as radiotracers. The radioisotopes in the molecules are particle emitters capable of depositing high energy within the vicinity of the decay sites. α and β^- emitters are well-known in tumour-targeted treatment but Auger-electron emitters are now being used or considered for therapeutic purposes [1–4]. In contrast to α and β^- radiotherapy, Auger-electron-based treatment requires targeting of radioisotopes into individual cells and even into the nucleus of these cells as optimal efficacy of the treatment is obtained when Auger emitters are tightly bound to DNA [2].

Tumour-targeted therapy based on Auger electrons is appealing because of its selective toxicity for target cells. Contrary to α and β^- radiation, Auger emitters remain low in toxicity while travelling in blood or bone marrow but become highly toxic when they are incorporated into the DNA of target cells [2]. Previous studies have demonstrated the superior cell killing efficacy of Auger emitters over β^--emitters in small tumours [5–7].

Historically, many experiments focus on the use of common medical Auger emitters such as ^{99m}Tc, ^{111}In and $^{123-125}$I. Experimental data on Auger emitters is scarce but calculated Auger yields of these common Auger emitters have been published by various authors [8–15]. However, there is a large scatter in the literature data for these common radioisotopes, and available data for exotic Auger emitters is meagre. In the past few years, a group of exotic Auger emitters, including ^{71}Ge, ^{140}Nd, ^{165}Er, and ^{155,161}Tb, which have more suitable half-lives and purer nuclear decays, is being considered and used for in vivo experiments [16–18]. There is a real need for new calculations of all relevant Auger emitters to assist research into Auger electrons and their applications.

Other than medical applications, the emission of Auger electrons has a role in nuclear physics. The average ionic charges of fission products are known to be shifted higher due to the emission of Auger electrons following nuclear decay of short-lived isomeric states in secondary fission fragments [19, 20]. Models of the Auger-electron emission can be used to calculate the charge-state distribution of residual ions due to the emission of Auger electrons to understand the experimental results.

In this paper, we compare the Auger yields of six medical radioisotopes, calculated by a Monte Carlo model that has been developed at the ANU, to the previous calculations. We also discuss the progress we have made with the Multiconfiguration Dirac-Hartree-Fock (MCDHF) method using the relativistic atomic structure packages: GRASP2K [21] and RATIP [22].

2 Production of Auger electrons

Auger electrons and X-rays are collectively named as atomic radiation. They are emitted from the atom after an atomic vacancy is created, either by artificial processes or natural phenomena. Detailed reviews of the production of Auger electrons and X-rays due to the creation of vacancy by natural decay can be found elsewhere [23–25].

3 Monte Carlo model of Auger cascade

Recognising the lack of a consistent theoretical model for the Auger cascade, the August 2011 IAEA special meeting on Intermediate-term Nuclear Data Needs for Medical Applications [28] concluded that: *"A comprehensive calculational route also needs to be developed to determine the energies and emission probabilities of the low-energy X-rays and Auger electrons to a higher degree of detail and consistency than is available at present."* A new approach is required, which should use theoretical transition energies and rates suited for the multiply ionized atoms. A model of the Auger cascade, which is based on a Monte Carlo method, has been developed as a first step to address the need.

Nuclear structure data is extracted from the **E**valuated **N**uclear **S**tructure **D**ata **F**ile (ENSDF) [29]. ENSDF is

[a] e-mail: boon.lee@anu.edu.au

maintained regularly and this will ensure the initial vacancy distribution is calculated with the latest evaluated nuclear data. Fractional electron capture probabilities for allowed and non-unique first forbidden transitions are calculated using an algorithm derived by Schönfeld [30]. Capture probabilities of other forbidden transitions are currently estimated with the same algorithm. These transitions are mostly low in intensity but there are some cases wherein they have a similar strength as the allowed transitions (for example, ^{124}I). Internal conversion coefficients (ICC) are calculated using the latest ICC calculator, BrIcc [31].

Atomic transition probabilities, which are calculated using the single-vacancy approximation, are taken from the **E**valuated **A**tomic **D**ata **L**ibrary (EADL) [32]. Chen *et al.* [33] demonstrated that discrepancies between values from EADL and experimental data are large in KLL transitions for elements with Z<60. Therefore, we replaced the KLL transition probabilities with theoretical values calculated in the relativistic intermediate coupling scheme with configuration interaction [33]. Since all atomic transition probabilities are calculated based on the single-vacancy approximation, an empirical correction, first used by Krause and Carlson [34], is applied to scale them by taking into consideration the realistic vacancy distribution. Examples of this correction can be found in Fig. 3 in Ref. [8].

The Auger cascade is a multi-step process, releasing one atomic radiation in each step. The energy of a transition at the N^{th} step is calculated using the following relation:

$$E^{A|X}|_N = E_T^{N+1} - E_T^N \qquad N \in [0, N_{max}]\,, \tag{1}$$

where $E^{A|X}$ denotes the energy of the emitted atomic transition and E_T^N is the total energy of the bound electrons at the N^{th} step. The atomic state *right after* a nuclear decay is labelled as N=0. At each N step, *ab initio* calculations of the total energy using the RAINE code [35], which is based on the relativistic Dirac-Fock (DF) method, are performed for states in both the N^{th} and N+1th steps. Energies of all possible transitions into a selected vacancy are calculated before a transition is selected. The sum of the probabilities of the energetically allowed transitions is then normalized to unity. This approach eliminates the transitions with negative energy from the selection pool.

When there are multiple coexisting vacancies, the following protocol is adopted:

1. Energies of all possible transitions into each vacancy are calculated. Energetically forbidden transitions are discarded.

2. Probabilities of remaining transitions are scaled by the Krause and Carlson correction. The sum of these probabilities is the total width of the vacancy.

3. The sum of all widths is then normalized to unity.

4. A random number is generated to select a vacancy to proceed in the Auger cascade. Another random number is then used to choose a kinematically allowed transition to this vacancy.

This protocol ensures that only the allowed transitions are taking part in the Auger cascade.

In all practical cases, we assume that the IC process and its associated Auger cascade take place *after* the daughter atom is fully neutralized following the atomic relaxation initiated by the EC decay. This assumption is not valid in rare cases wherein the nuclear level half life of the daughter nucleus is comparable to the life-time of the Auger cascade. An example of these rare cases is discussed in Ref. [23].

There are two approaches in dealing with valence vacancies built up in the Auger cascade. The first approach is to neutralize any vacancies created in the valence shell during the Auger cascade. This is known as *fast* neutralisation. In this approach, if the transition probabilities from all non-valence subshells are known, the atom is completely neutralized at the end of the Auger cascade. For ^{125}I decay, the O-shell is the valence shell and the transition probabilities from the K-shell up to N_5-subshell are available from the EADL [32], the residual tellurium atom will be fully neutralized. In order to address the fate of the potential energy associated with residual charge, it is considered that these vacancies will be filled by the electrons directly from the continuum, with the emission of X-rays. The second approach is termed as *slow* neutralisation as no vacancies are neutralized during the short lifetime of the Auger cascade. Results from both approaches are listed in Table 1.

Calculated charge-state distributions, in the *slow* neutralisation approach, agree well with experimental data in the rare gases only if shake-off transitions are included (data not shown). This indicates that radiative and non-radiative transitions alone, are not sufficient to describe the Auger cascade. Nevertheless, small probabilities of shake-off and double-Auger transitions are ignored in our work to date due to the lack of data for elements other than the rare gases.

4 Multiconfiguration Dirac-Hartree-Fock method

Recent analyses show that some other computational methods appear to be more accurate than the method used in EADL [36]. Moreover, some errors in tabulating the library have been detected [37]. Calculations of Auger yields are extremely sensitive to the input cross sections. Inaccurate atomic transition probabilities from EADL will dominate the uncertainties in the calculated Auger yields.

Therefore, we aim to replace the atomic cross sections from EADL using the relativistic atomic structure packages, namely the **G**eneral **P**urpose **R**elativistic **A**tomic **S**tructure **P**rogram, GRASP2K [21] and the **R**elativistic **A**tomic **T**ransition and **I**onization **P**roperties, RATIP [22]. These programs are based on the relativistic Multiconfiguration Dirac-Hartree-Fock (MCDHF) method.

In this paper, ^{85}Rb is investigated due to the availability of experimental data. For an electron-capture-triggered K-hole in ^{85}Rb, the possible KLL-Auger decay processes are given by

$$\begin{aligned} {}^{85}\mathrm{Rb}^*(1s^1 5s^2) &\rightarrow {}^{85}\mathrm{Rb}^*(2s^0 5s^2) + e_A^- \\ &\rightarrow {}^{85}\mathrm{Rb}^*(2s^1 2p^5 5s^2) + e_A^- \\ &\rightarrow {}^{85}\mathrm{Rb}^*(2p^4 5s^2) + e_A^- \end{aligned} \quad (2)$$

where e_A^- is a KLL Auger electron. Calculations of the initial, and final states of the transitions given by Eq (2) were carried out using the MCDHF method by applying the GRASP2K code [21] in the extended optimal level (EOL) scheme [38], where optimization is on a weighted sum of energies, together with the RELCI extension [39]. Detailed descriptions of MCDHF can be found elsewhere (see Parpia *et al* [40] and references therein). Therefore, only the main principles are reviewed here. In the MCDHF method, the atomic state function (ASF) is represented as a superposition of jj-coupled configuration state functions (CSF) of the type

$$\Psi(\nu PJM_J) = \sum_{j=1}^{n_c} c_j \Phi(\nu_j PJM_J), \quad (3)$$

where Ψ and Φ are, respectively, the ASF and CSF; P, J, and M_J are the relevant quantum numbers: parity, total angular momentum, and its associated total magnetic quantum number, respectively; ν stands for all the other quantum numbers that are necessary to describe the ASFs and CSFs, for example orbital occupancy and coupling scheme. The summation in Eq (3) is up to n_c, the number of CSFs in the expansion, and each CSF is built from antisymmetrized products of the one-electron Dirac orbitals, represented on some numerical mesh, for which initial estimates were obtained using the Thomas-Fermi model. In the relativistic self-consistent field procedure, both the expansion coefficients, c_j, and the radial parts of the Dirac orbitals are optimized to self-consistency on the basis of the Dirac-Coulomb Hamiltonian

$$H_{DC} = \sum_i h_D(\mathbf{r_i}) + \sum_{i>j} \frac{1}{r_{ij}} \quad (4)$$

In the Hamiltonian (4), $h_D(\mathbf{r})$ denotes the standard one-electron Dirac Hamiltonian in the field of the nucleus. The Breit interaction and the vacuum polarization are included in subsequent relativistic configuration interaction (RCI) calculations (RELCI) [39].

The AUGER component [41] of the RATIP package [22] has been adopted to calculate the Auger transition energies and rates. In this component, a central-field approximation has been adopted to treat the interaction of the outgoing electron with the bound-state electron density. This results in continuum spinors which are obtained independently for each final state of the K-Auger decay process within a spherical but level-dependent potential of the final ion (the so-called *optimal level* scheme). This component also incorporates the exchange interaction of the emitted electron with the bound electrons.

5 Results & Discussion

Table 1 compares the calculated Auger-electron yields of six medical radioisotopes, namely ^{71}Ge, ^{99m}Tc, ^{111}In, and $^{123-125}$I, to the previous calculations. The table reports updated Auger-electron yields compared to the previously published values in [23–25] for the four radioisotopes other than ^{71}Ge and ^{124}I. In the present work, all calculations are taking 10^5 Monte Carlo events into consideration. Calculations in the Table 1 follow two fundamentally different approaches to evaluate the Auger cascade, designated 'deterministic' and 'Monte Carlo'. A detailed review of these two approaches has been given elsewhere [9, 23, 24].

The Auger-electron yields from the RADAR [11] and DDEP [27] evaluations are much lower than the other tabulations because they do not include low-energy transitions. Their approach could lead to wrong estimation of absorbed doses in dosimetry and microdosimetry using medical radioisotopes. The approach adopted by Stepanek *et al* [9, 10] and Pomplun [13, 14] is closer to the one adopted in our work as these authors calculate transition energies quantum mechanically. In contrast, Eckerman and Endo [12], Howell [8], and Nikjoo [15] used the $Z/Z+1$ rule [44] to estimate transition energies.

The calculated Auger yields from Eckerman and Endo are consistent with values from Howell, except for ^{111}In. A difference of 7.48 can be attributed to the exclusion of NXY Auger transitions in the Eckerman and Endo model.

The differences between the Auger-electron yields of ^{99m}Tc and ^{111}In, calculated using the *fast* and *slow* neutralization in our work, are smaller than the other radioisotopes. This could be due to the exclusion of transitions from the $N_{4,5}$-subshells in the EADL. However, Stepanek *et al* [10] demonstrated that the inclusion of transitions into the $N_{4,5}$- and $O-$subshells, estimated using the Kassis rule [45], did not increase the calculated Auger yield of ^{111}In. They concluded that these outer-shell transitions become energetically forbidden during the Auger cascade, if the transition energies are calculated by means of a quantum-mechanical method.

Although the approach adopted by Stepanek is close to our work, his model yielded a lower number of electrons. The extra electrons in our calculation are coming from the outer-shell transitions listed in the EADL [32]. The difference can be attributed to the different approaches in removing forbidden transitions. Stepanek was using a rejection method to eliminate kinematically impossible transitions. In contrast, the current model has eliminated all energetically forbidden transitions before a vacancy is selected to propagate. Thus some propagations were not utilized in Stepanek's model, resulting in less outer-shell transitions.

Table 1 shows that our work agrees very well with the Nikjoo values in the *fast* neutralisation approach. The calculated Auger yields are also consistent with the Howell values if the outer-shell transitions estimated using the

Table 1. Calculated Auger electron yield per nuclear decay for selected medical radioisotopes.

	RADAR[a,c] [11, 26]	DDEP[a,c] [27]	Eckerman & Endo[a,d] [12]	Howell[b,d] [8]	Stepanek[b,d] [9, 10]	Pomplun[b,e] [13, 14]	Nikjoo[b,d] [15]	This work[b,e]	This work[b,d]
^{71}Ge	1.65							3.98	4.88
^{99m}Tc	0.12	0.13	4.38	4.0		2.5[f]		3.52	3.89
^{111}In	1.14	1.16	7.22	14.7	6.05	5.63[g]		5.92	6.40
^{123}I	1.06	1.08	13.7	14.9		6.4[f]		7.41	12.4
^{124}I	0.71		1.96 [h]				8.2	5.04	8.40
^{125}I	1.77	1.78	23.0	24.9	14.5	12.2	20.2	11.8	20.1

[a] Deterministic.
[b] Monte Carlo.
[c] Only transitions from K- and L-shells are considered.
[d] Fast neutralization.
[e] Slow neutralization.
[f] Shake-off electron is included. ^{99m}Tc : 0.5, ^{123}I : 0.9.
[g] Published in Stepanek *et al.* [10].
[h] N-shell transitions are excluded.

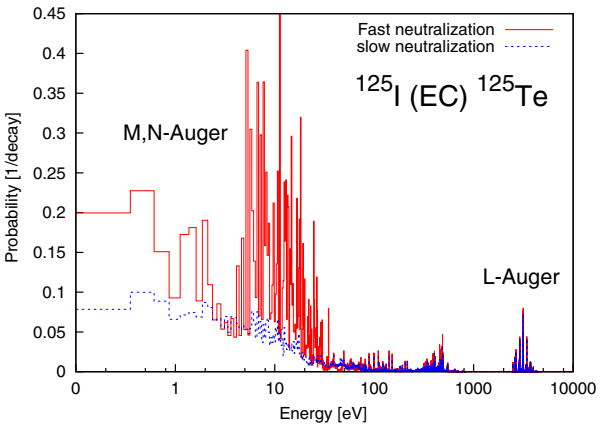

Figure 1. Comparison between the low-energy Auger spectra of ^{125}I decay calculated using the fast and slow neutralization. Energy-bin of 0.25 eV is applied to both spectra.

Kassis rule are taken out from Howell's model. Nevertheless, the calculated average energies of N-shell transitions are much lower than Howell's values as we computed the energies quantum mechanically, taking into account the spectator vacancies, in contrast to the $Z/Z+1$ rule he adopted. This indicates that the Auger yields calculated from the relativistic DF method are consistent with the results estimated using $Z/Z+1$ rule only if the transitions listed in the EADL are included. More investigations are needed to quantify the effect of the realistic vacancy distribution on the energies and yields of the outer-shell transitions deduced from the Kassis rule.

The calculated number of electrons per decay using the *slow* neutralisation approach in this work agrees with the values from Pomplun's model. Pomplun included shake-off transitions in his calculations but the reference he used for the shake-off probabilities only contains values for rare gases. It is unclear what method was used to obtain the shake-off rates for transition metals like technetium.

Figure 1 shows the difference between the low-energy Auger spectra of tellurium following the decay of ^{125}I calculated using two different approaches. The two spectra are very similar for energies above 100 eV but the intensities of low-energy electrons in the fast neutralization are much higher than the slow neutralization. Within some energy-bins, the intensities of electrons in the fast neutralization are about four times bigger than their counterparts.

Figure 2 compares the theoretical KLL spectrum calculated by the MCDHF method to the experimental data collected from the EC decay of ^{85}Sr to ^{85}Rb. Except for the KL_1L_1 ($^1S_0$) and KL_1L_2 ($^1P_1$) transitions, excellent agreement between theoretical KLL components and the experimental spectrum, in both the energies and intensities, is achieved. The disagreement for the two lower-energy transitions is currently unexplained. One possible reason is the exclusion of correlated electron-orbitals in the calculation.

6 Future directions

The MCDHF method is able to deliver more accurate transition intensities and energies than the EADL [32] and the RAINE [35] code. We aim to, in the next step, replace the transition intensities from the EADL [32] with MCDHF values calculated for single-vacancy atoms. This will improve the accuracy of Auger yields since the transition intensities calculated by the MCDHF method are more accurate than the ones tabulated in the EADL. Furthermore, the

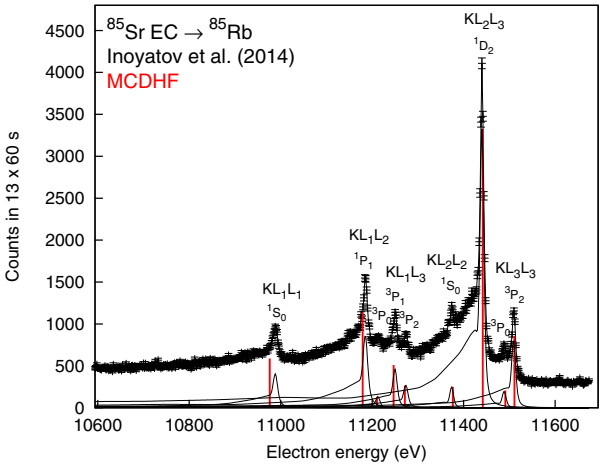

Figure 2. KLL Auger spectrum calculated using the MCDHF method is compared to experimental data from Ref. [42]. Spectral profile of individual component (in solid line) is evaluated from the measured spectrum using the computer code described in Ref. [43].

MCDHF method will be able to calculate transitions for all subshells from the first principles. In contrast, the EADL has missing transitions between some outer-subshells.

Lowe *et al* [46] demonstrated some success in *ab initio* calculations of the shake-off probabilities for transition-metals using the GRASP2K code. The shake-off transitions will be incorporated into our model if consistent calculations can be achieved. It is also possible to validate (or otherwise) the Krause and Carlson correction by applying the MCDHF method in multiply-ionized systems.

7 Conclusion

The ultimate aim of this work is to create a Monte Carlo program to simulate the Auger cascade and hence calculate the Auger yields and charge-state distributions by a consistent and reliable method. Better access to the Auger spectra in both the *fast* and *slow* neutralization approaches through the program will benefit research in both the physical and medical applications. Calculated Auger spectra, which account for kinematically forbidden transitions by computing transition energies using the relativistic Dirac-Fock (DF) method, agree with the previous calculations that used the $Z/Z+1$ rule to estimate transition energies for transitions listed in the EADL [32]. More investigations are needed to quantify the effect of using a realistic vacancy distribution for the transitions between outer-shells, that are missing from the EADL.

Progress has been made with the Multiconfiguration Dirac-Hartree-Fock (MCDHF) method to calculate the KLL Auger spectrum of rubidium. Excellent agreement in both the energies and intensities of KLL components with the experiment is achieved except for the KL$_1$L$_1$ (^{1}S$_0$) and KL$_1$L$_2$ (^{1}P$_1$) transitions. This indicates that the use of the MCDHF method will improve the input cross sections of the model and thus improve the accuracy of its results.

Acknowledgements

This work is supported by Australian Research Discovery grant DP140103317. The authors would like to thank A. Kovalík and A. Inoyatov of the Laboratory of Nuclear Problems, JINR, for providing the experimental data on the ^{85}Sr decay and P. Jönsson and J. Ekman of Malmö University for helping with the use of GRASP2K and RATIP.

References

[1] D. J. Kwekkeboom *et al*, J. Nucl. Med. **46**, 62S (2005).
[2] F. Buchegger *et al*, Eur J. Nucl. Med. Mol. Imaging. **33**, 1352 (2006).
[3] D. J. Kwekkeboom *et al*, Eur. J. Nucl. Med. Mol. Imaging **23**, 417 (2003).
[4] C. Waldherr *et al*, J. Nucl. Med. **43**, 610 (2002).
[5] R. B. Michel *et al*, J. Nucl. Med. **44**, 632 (2003).
[6] T. M. Behr *et al*, Eur. J. Nucl. Med. **27**, 753 (2000).
[7] S. V. Govindan *et al*, J. Nucl. Med. **41**, 2089 (2000).
[8] R. W. Howell, Med. Phys. **19**, 1371 (1992).
[9] J. Stepanek, Med. Phys. **27**, 1544 (2000).
[10] J. Stepanek, Acta Onco. **39**, 667 (2000).
[11] M. G. Stabin *et al*, Health. Phys. **83**, 471 (2002).
[12] K.F. Eckerman *et al*, Soc. Nucl. Med. (2007).
[13] E. Pomplun, Acta. Oncol. **39**, 673 (2000).
[14] E. Pomplun, Int. J. Radiat. Biol. **88**, 108 (2012).
[15] H. Nikjoo *et al*, Int. J. Radiat. Biol. **84**, 1011 (2008).
[16] S. Lehenberger *et al*, Nucl. Med. Biol. **38**, 917 (2011).
[17] C. Müeller *et al*, J. Nucl. Med. **53**, 1951 (2012).
[18] C. Müeller *et al*, Eur. J. Nucl. Med. Mol. Imaging **41**, 476 (2014).
[19] H. Wohlfarth *et al*, Z. Phys. A **287**, 153 (1973).
[20] T. Rzaca-Urban *et al*, Phys. Rev. C **80**, 064317 (2009).
[21] P. Jonsson *et al*, Comput. Phys. Commun. **184**, 2197 (2013).
[22] S. Fritzsche, Comput. Phys. Commun. **183**, 1525 (2012) .
[23] B. Lee *et al*, Comput. Math. Meth. Med. **14**, 651475 (2012).
[24] B. Lee *et al*, Eur. Phys. J. : Web of Conferences **35**, 04003 (2012).
[25] B. Lee *et al*, Eur. Phys. J. : Web of Conferences **63**, 01002 (2013).
[26] RAdiation Dose Assessment Resource (RADAR), http://www.doseinfo-radar.com/RADARHome.html.
[27] Decay Data Evaluation Project, http://www.nucleide.org/DDEP_WG/DDEPdata.htm, ^{99m}Tc: C. Morillon, M. M. Bé, A. Egorov (2012); ^{111}In: V. P. Chechev (2006); ^{123}I: V. Chiste, M. M. Bé (2004); ^{125}I: V. Chiste, M. M. Bé (2010).
[28] Summary Report of the "Technical Meeting on Intermediate-term Nuclear Data Needs for Medical Applications: Cross Sections and Decay Data", INDC International Nuclear Data Committee, Eds. A. L.

Nichols, S. M. Qaim, R. C. Noy, INDC(NDS)-0596, September (2011).
[29] Evaluated Nuclear Structure Data File (ENSDF), NNDC, BNL http://www.nndc.bnl.gov/ensdf/index.jsp.
[30] E. Schönfeld, Appl. Radiat. Isot. **49**, 1353 (1998).
[31] T. Kibédi *et al*, Nucl. Instr. and Meth. in Phys. Res. A **589**, 202 (2008).
[32] S. T. Perkins *et al*, LLNL, UCRL **30** (1991).
[33] M. H. Chen *et al*, Phys. Rev. A, **21**, 442 (1980).
[34] M. O. Krause *et al*, Phys. Rev. **158**, 28 (1967).
[35] I. M. Band *et al*, At. Data Nucl. Data Tables **81**, 1 (2002).
[36] M. G. Pia *et al*, IEEE Trans. Nucl. Sci. **56**, 3650 (2009).
[37] A. Lechner *et al*, IEEE Nucl. Sci. Symp. Conf. Rec., 2869 (2008).
[38] K. G. Dyall *et al*, Comput. Phys. Commun. **55**, 425 (1989).
[39] S. Fritzsche *et al*, Comput. Phys. Commun. **148**, 103 (2002).
[40] F. A. Parpia *et al*, Comput. Phys. Commun. **94**, 249 (1996).
[41] S. Fritzsche, J. Electron Spectrosc. Relat. Phenom. **114**, 1155 (2001).
[42] A. Inoyatov *et al*, Phys. Scr. **90**, 025402 (2015) .
[43] A. Inoyatov *et al*, J. Electron Spectrosc. Relat. Phenom. **160**, 54 (2007).
[44] M. F. Chung *et al*, Surface Science **22**, 479 (1970).
[45] A. I. Kassis *et al*, J. Nucl. Med. **24**, 1164 (1983).
[46] J. A. Lowe *et al*, Phys. Rev. A **83**, 060501 (2011).